One- and many-electron self-interaction error in local and global hybrid functionals

Tobias Schmidt and Stephan Kümmel*
Theoretical Physics IV, University of Bayreuth, 95440 Bayreuth, Germany
(Received 19 January 2016; revised manuscript received 22 March 2016; published 14 April 2016)

Electronic self-interaction poses a fundamental challenge in density-functional theory. It greatly limits, e.g., the physical interpretation of eigenvalues as electron removal energies. We here investigate whether local hybrid functionals that are designed to be free from one-electron self-interaction lead to occupied Kohn-Sham eigenvalues and orbitals that approximate photoemission observables well. We compare the local hybrid results to the ones from global hybrid functionals that only partially counteract the self-interaction, and to the results that are obtained with a Perdew-Zunger-type self-interaction correction. Furthermore, we check whether being nominally free from one-electron self-interaction translates into a reduced many-electron self-interaction error. Our findings show that this is not the case for the local hybrid functionals that we studied: In practice they are similar to global hybrids in many respects, despite being formally superior. This finding indicates that there is a conceptual difference between the Perdew-Zunger way and the local hybrid way of translating the one-electron condition to a many-electron system. We also point out and solve some difficulties that occur when using local hybrid functionals in combination with pseudopotentials.

DOI: 10.1103/PhysRevB.93.165120

I. INTRODUCTION

Due to its favorable balance between accuracy and numerical efficiency, Kohn-Sham density-functional theory (DFT) [1,2] has become the standard method for electronic structure calculations. Based on the electron density $n(\mathbf{r})$ as the central quantity, DFT provides an elegant and in principle exact framework to solve the quantum-mechanical many-body problem [3–5].

In practice, the quality of the results from a DFT calculation decisively depends on the approximation to the exchange-correlation (xc) energy $E_{\mathrm{xc}}[n]$. From the early years of DFT on, there was a strong focus of research on developing reliable density functional approximations. This research led to functionals that successfully describe a range of physical ground-state properties [6]. Even long-known (semi)local functionals such as the local spin density approximation (LSDA) [7–9] or the PBE generalized gradient approximation [10,11] often yield reliable binding energies and structures. Yet, DFT use and research also uncovered many deficiencies of these established approximations. On the one hand there are numerous limitations in quantitative accuracy. On the other hand there are also qualitative problems. Among them are the erroneous dissociation behavior of diatomic radicals [12–15] and neutral molecules [16–21] and the drastic overestimation of static electric polarizabilities and hyperpolarizabilities of molecular chains [22–27]. The approximate interpretation of Kohn-Sham eigenvalues and orbitals as photoemission observables is of great practical interest, yet also problematic (see, e.g., Refs. [28–36] and references therein). When using common functionals in time-dependent DFT, e.g., via an adiabatic approximation, further difficulties arise, in particular with respect to charge-transfer excitations [37–40] and electronic transport characteristics [41–44].

This diverse set of issues in practical DFT can be traced back to a common conceptual problem: electronic self-interaction (SI). SI can be understood by the example of a single-electron system with ground-state density $n^{1\mathrm{e}}(\mathbf{r})$. In this case, the Hartree energy E_{H} has to be fully canceled by E_{xc}, i.e., $E_{\mathrm{H}}[n^{1\mathrm{e}}] + E_{\mathrm{xc}}[n^{1\mathrm{e}}] = 0$, since otherwise one obtains an erroneous interaction of the electron with itself, the SI error (SIE) [45].

For a system with more than one electron, it is less obvious how to quantify the SIE. The most famous definition for a system with $N = \sum_\sigma N_\sigma$ electrons being free from SIE [45,46] is based on identifying orbitals with electrons [47]. When making this identification, which goes beyond the usual Kohn-Sham concept and in principle raises the question of whether orbital densities are allowed to be inserted into the ground-state energy functional despite them not being ground-state densities [48], then the electrons are represented by the spin-orbital densities $n_{i\sigma}(\mathbf{r}) = |\varphi_{i\sigma}(\mathbf{r})|^2$ of the occupied Kohn-Sham orbitals $\varphi_{i\sigma}(\mathbf{r})$. With this identification, the famous Perdew-Zunger definition

$$\sum_{\sigma=\uparrow,\downarrow} \sum_{i=1}^{N_\sigma} \left\{ E_{\mathrm{H}}[n_{i\sigma}] + E_{\mathrm{xc}}^{\mathrm{approx}}[n_{i\sigma}, 0] \right\} = 0 \tag{1}$$

appears as a very natural concept. Here, i counts the Kohn-Sham states and σ the electron spin. As this definition is directly linked to the single-electron case, a functional fulfilling $E_{\mathrm{H}}[n^{1\mathrm{e}}] + E_{\mathrm{xc}}[n^{1\mathrm{e}}] = 0$ for any $n^{1\mathrm{e}}(\mathbf{r})$, ore more generally Eq. (1), is referred to as being free from the one-electron self-interaction error. For brevity, we denote the one-electron self-interaction error as *one-error* in the following.

However, as orbital densities cannot always be identified with electrons, Eq. (1) does not unambiguously quantify the SI problem. The more general concept of the many-electron self-interaction error (in the following referred to as *many-error*) [14,17] uses the straight-line energy condition [49] to define the SIE in a many-electron system in a different way. A functional is defined as being free from many-error if the total energy $E(N)$ of an N electron system is piecewise linear as a function of particle number,

$$E(N) = (1-\omega)E(N_0) + \omega E(N_0+1), \tag{2}$$

*stephan.kuemmel@uni-bayreuth.de

with $N = N_0 + \omega$, where $N_0 \in \mathbb{N}$ gives the number of electrons in the singly ionized system and $w \in [0,1[$ denotes the fraction of an electron that is added. The many-error is often referred to as delocalization error, since the SI leads to a spurious delocalization of the charge distribution [50]. It is well established that standard, (semi)local functionals show a convex, while Hartree-Fock (and pure exact exchange as defined below) gives a concave energy curve [14,51,52].

Although systems with a fractional number of electrons seem like rather abstract constructions, the implications of a functional violating Eq. (2) are of direct physical relevance. Especially the problem of predicting fundamental gaps from Kohn-Sham eigenvalues is connected to the deviation from piecewise linearity in the energy curves of the employed functional [52–56]. Furthermore, it was demonstrated that it is the violation of Eq. (2) that leads to the aforementioned incorrect description of molecular dissociation, because solutions with fractional charges on separate atoms incorrectly become energetically favorable [13,15,17,57–59].

In light of the problems caused by electronic SI, much effort has been invested in addressing both the one- and the many-error. Equation (1) sets the basis for SI correction (SIC) schemes, that, by explicitly removing the one-error from SI affected functionals, remedy the aforementioned shortcomings to a large extent (see Ref. [60] and references therein for a detailed discussion). Using SIC methods, e.g., electrical response properties of molecular chains were predicted more accurately [25,61], and the description of charge transport characteristics [41,44] and charge-transfer excitations [40] was qualitatively improved.

The recently proposed ensemble generalization of DFT [52] addresses the many-error. Restoring piecewise linearity to a large extent, its application leads to a better description of ionization potentials (IPs) [56] and fundamental gaps using Kohn-Sham eigenvalues [55], and eliminates fractional dissociation [59].

A different approach to counteract SI is based on using exact exchange (EXX). EXX is defined as the Fock exchange integral evaluated with Kohn-Sham orbitals,

$$E_{\mathrm{x}}^{\mathrm{ex}} = -\frac{1}{2} \sum_{\substack{i,j=1 \\ \sigma=\uparrow,\downarrow}}^{N_\sigma} \iint \frac{\varphi_{i\sigma}^*(\mathbf{r})\varphi_{j\sigma}(\mathbf{r})\varphi_{i\sigma}(\mathbf{r}')\varphi_{j\sigma}^*(\mathbf{r}')}{|\mathbf{r}-\mathbf{r}'|} \mathrm{d}^3r\, \mathrm{d}^3r'. \tag{3}$$

EXX fulfills the condition (1) and is thus a natural "ingredient" in functional constructions that try to address SI.

Global hybrid functionals [62–64], as motivated by the adiabatic connection [65–67], use a fixed, constant amount of EXX in combination with (semi)local functional components. This leads to a considerable improvement over purely (semi)local functionals for ground-state properties if about 25% of EXX are used. However, global hybrids with such a parametrization often perform less well than, e.g., SIC schemes, in situations that are known to be strongly influenced by electronic SI. The reason for this is presumably that global hybrid functionals with a small fraction of EXX are not one-error free.

Local hybrid functionals [68–71] take the idea of combining nonlocal and (semi)local functional parts one step further. Based on the concept of (nonuniquely [71–73]) expressing the xc energy via the integral $E_{\mathrm{xc}}[n] = \int n(\mathbf{r})\, e_{\mathrm{xc}}(\mathbf{r})\, \mathrm{d}^3r$, they approximate the xc energy density per particle $e_{\mathrm{xc}}(\mathbf{r})$ as a spatially resolved mix of nonlocal and (semi)local components. Local hybrids proved to be a powerful functional ansatz for the description of thermochemistry and reaction barriers [70,74–85] and appear promising in linear-response time-dependent DFT [86].

The local hybrids' mixing concept provides for much more flexibility in the functional construction than the global hybrids' fixed fraction of exchange. Consequently, the two types of functionals typically differ substantially in the formal treatment of the SIE: In contrast to global hybrids, local hybrids can be constructed to be inherently free from the one-error in the sense of Eq. (1) [69,87,88]. Yet, despite this important conceptual difference, local and global hybrids share more features than one would intuitively expect. One of them is the recently discussed incorrect asymptotic decay of the local xc potential [89].

In the present paper, we systematically investigate the differences and similarities that exist between local and global hybrid functionals with respect to the SIE. In Sec. II we review the global and local hybrid functionals that we employ in this study. In Sec. III we present some insights on the influence of SI on the description of physical quantities. Section IV provides details of our calculations. In Sec. V A we contrast manifestations of the one-error in calculations using global and local hybrids to the ones found in calculations using full SIC schemes. We focus on the interpretability of DFT eigenvalues and orbitals as photoemission observables. In Sec. V B we study the connection between the one- and many-error for global and local hybrids with the help of total energy curves $E(N)$ for fractionally charged systems. In our concluding Sec. VI we discuss the implications that our findings have for the construction and use of functionals that are only nominally free from the one-error.

II. THE INVESTIGATED FUNCTIONALS

We use the PBEh functional [90,91] as a representative for global hybrid functionals. Employing a constant amount $a \in [0,1]$ of the EXX energy density $e_{\mathrm{x}}^{\mathrm{ex}}(\mathbf{r})$ as (implicitly) defined by Eq. (3) together with corresponding amounts of PBE xc energy densities $e_{\mathrm{x,c}}^{\mathrm{PBE}}(\mathbf{r})$, it approximates the overall xc energy density per particle by

$$e_{\mathrm{xc}}^{\mathrm{PBEh}}(a,\mathbf{r}) = a\, e_{\mathrm{x}}^{\mathrm{ex}}(\mathbf{r}) + (1-a)\, e_{\mathrm{x}}^{\mathrm{PBE}}(\mathbf{r}) + e_{\mathrm{c}}^{\mathrm{PBE}}(\mathbf{r}). \tag{4}$$

While PBEh with $a \approx 0.25$ performs well for binding energies, $a \approx 0.75$ leads to [92–94] highest occupied (ho) Kohn-Sham eigenvalues that approximate experimental IPs well via the IP theorem, i.e., $I = -\varepsilon_{\mathrm{ho}}$ [49,95–98]. In the following, we explore how this functional's performance with respect to the one- and many-error depends on the value of a.

As a representative for the local hybrid functionals we use the "ISO-functional" introduced in Ref. [88]. It replaces the mixing constant a by a spatially resolved local mixing function (LMF) $(1 - f_{\mathrm{x}}[n](\mathbf{r}))$ and introduces a separate LMF $f_{\mathrm{c}}[n](\mathbf{r})$ for the correlation part:

$$e_{\mathrm{xc}}^{\mathrm{ISO}}(c,\mathbf{r}) = (1 - f_{\mathrm{x}}[n](\mathbf{r}))\, e_{\mathrm{x}}^{\mathrm{ex}}(\mathbf{r}) + f_{\mathrm{x}}[n](\mathbf{r})\, e_{\mathrm{x}}^{\mathrm{LSDA}}(\mathbf{r}) + f_{\mathrm{c}}[n](\mathbf{r})\, e_{\mathrm{c}}^{\mathrm{LSDA}}(\mathbf{r}), \tag{5}$$

where the LMFs are given by

$$f_{\mathrm{x}}[n](c,\mathbf{r}) = \frac{1-\frac{\tau_{\mathrm{W}}(\mathbf{r})}{\tau(\mathbf{r})}\zeta^2(\mathbf{r})}{1+ct^2(\mathbf{r})} \tag{6}$$

and

$$f_{\mathrm{c}}[n](\mathbf{r}) = 1-\frac{\tau_{\mathrm{W}}(\mathbf{r})}{\tau(\mathbf{r})}\zeta^2(\mathbf{r}). \tag{7}$$

Here, $\tau_{\mathrm{W}}(\mathbf{r}) = |\nabla n(\mathbf{r})|^2/(8n(\mathbf{r}))$ denotes the von Weizsäcker and $\tau(\mathbf{r}) = \frac{1}{2}\sum_\sigma \sum_{i=1}^{N_\sigma} |\nabla\varphi_{i\sigma}(\mathbf{r})|^2$ the Kohn-Sham kinetic energy density. The function $t^2(\mathbf{r})$ is the reduced density gradient [10]

$$t^2(\mathbf{r}) = \left(\frac{\pi}{3}\right)^{1/3}\frac{a_0}{16\Phi^2(\zeta(\mathbf{r}))}\frac{|\nabla n(\mathbf{r})|^2}{n^{7/3}(\mathbf{r})}, \tag{8}$$

with the Bohr radius a_0, $\Phi(\zeta(\mathbf{r})) = \frac{1}{2}((1+\zeta)^{2/3}+(1-\zeta)^{2/3})$ and the spin polarization $\zeta(\mathbf{r}) = (n_\uparrow(\mathbf{r})-n_\downarrow(\mathbf{r}))/(n_\uparrow(\mathbf{r})+n_\downarrow(\mathbf{r}))$. A detailed motivation and discussion of this functional was given in Refs. [88,89]. In the context of the present work it is important to be aware of three aspects.

First, the ISO-functional contains an initially undetermined parameter c in the denominator of Eq. (6). We recently demonstrated that $c \approx 0.5$ is optimal for binding energies, whereas $c \approx 5.0$ is best for predicting IPs via $\varepsilon_{-\mathrm{ho}}$. The parameter c determines the intrinsic amount of EXX in the ISO functional, i.e., in this sense corresponds to a in Eq. (3). The higher the value of c, the smaller $f_{\mathrm{x}}(\mathbf{r})$ generally gets, resulting in an intrinsically higher fraction of EXX.

Second, it can be shown that ISO obeys condition Eq. (1) *independently* of the value of c. Based on the fact that $\tau_{\mathrm{W}}(\mathbf{r})/\tau(\mathbf{r}) \to 1$ and $\zeta^2(\mathbf{r}) \to 1$ if evaluated on one-spin-orbital densities of ground-state character (see Ref. [89] for a more detailed discussion), both $f_{\mathrm{x}}(\mathbf{r})$ and $f_{\mathrm{c}}(\mathbf{r})$ in Eqs. (6) and (7) vanish, leaving only pure EXX in Eq. (5), and thus canceling the Hartree contribution completely. In this sense, in contrast to global hybrid functionals, the local hybrid ISO is free from one-error.

The third aspect regards the explicit occurrence of the spin polarization $\zeta(\mathbf{r})$ in the LMFs of ISO. This function was originally introduced in order to prevent the LMFs from incorrectly identifying regions in space that are dominated by two spatially identical orbitals with opposite spins as one electron regions. However, for fully spin-unpolarized systems $\zeta(\mathbf{r}) = 0\,\forall\,\mathbf{r}$. Thus, the detection function $\tau_{\mathrm{W}}(\mathbf{r})/\tau(\mathbf{r})$ in $f_{\mathrm{x}}(\mathbf{r})$ and $f_{\mathrm{c}}(\mathbf{r})$ is multiplied by zero for such systems. One therefore might argue that effectively the LMFs are not using the detection function, while at the same time Eq. (1) is undoubtedly fulfilled. Therefore, we here introduce a modification of the ISO functional without spin polarization. It uses the LMFs

$$f_{\mathrm{x}}^{\mathrm{II}}(c^*,\mathbf{r}) = \frac{1-\frac{\tau_{\mathrm{W}}(\mathbf{r})}{\tau(\mathbf{r})}}{1+c^*t_{\mathrm{II}}^2(\mathbf{r})} \tag{9}$$

and

$$f_{\mathrm{c}}^{\mathrm{II}}(\mathbf{r}) = 1-\frac{\tau_{\mathrm{W}}(\mathbf{r})}{\tau(\mathbf{r})}. \tag{10}$$

Here, $t_{\mathrm{II}}^2(\mathbf{r}) = t^2(\zeta(\mathbf{r})=1,\mathbf{r}) = (\frac{\pi}{3})^{1/3}\frac{a_0 2^{\frac{2}{3}}}{16}\frac{|\nabla n(\mathbf{r})|^2}{n^{7/3}(\mathbf{r})}$. Note that also this construction (called ISOII in the following) has an undetermined parameter, c^*. It plays a similar role as c does in ISO. The modified ISOII, in contrast to ISO, reduces the xc energy density to pure EXX also for two spatially identical orbitals, and both functionals are free from one-error in the sense of Eq. (1).

III. MANIFESTATIONS OF SELF-INTERACTION

The interpretation of occupied Kohn-Sham eigenvalues as a physical density of states (DOS), as frequently done to interpret experimental photoemission spectra, markedly illustrates the one-error. Even though only the ho Kohn-Sham eigenvalue is rigorously physically meaningful, it has been argued that also lower lying eigenvalues can be good approximations to electron removal energies [30,36,99,100]. However, the spectra obtained by standard functionals can be very much distorted due to electronic SI. In Ref. [32] the orbital self-interaction error (OSIE) was introduced as a criterion to quantify the influence of one-error on the eigenvalue structure. The OSIE is defined as

$$e_{i\sigma} = \langle\varphi_{i\sigma}|v_{\mathrm{H}}[|\varphi_{i\sigma}|^2]|\varphi_{i\sigma}\rangle + \langle\varphi_{i\sigma}|v_{\mathrm{xc}\sigma}[|\varphi_{i\sigma}|^2,0]|\varphi_{i\sigma}\rangle, \tag{11}$$

with $v_{\mathrm{H}}[|\varphi_{i\sigma}|^2](\mathbf{r})$ denoting the Hartree and $v_{\mathrm{xc}\sigma}[|\varphi_{i\sigma}|^2,0](\mathbf{r})$ the xc potential evaluated on single spin-orbital densities.

The OSIE is a valuable indicator for the quality of eigenvalue spectra. If Eq. (11) gives a different OSIE for all Kohn-Sham states, i.e., self-interaction affects different eigenvalues to a different degree, then a completely distorted spectrum is to be expected and the DOS will not even qualitatively reflect the spectrum that is observed in a photoemission experiment [32,33,100–102].

Evaluating Eq. (11) with an explicitly density-dependent functional is straightforward, but calculating $e_{i\sigma}$ for an explicitly orbital-dependent functional is more difficult. The problem is that no explicitly density-dependent expression for $v_{\mathrm{xc}\sigma}$ exists that could be directly evaluated on a single spin-orbital density. However, also for orbital-dependent functionals the following relation holds:

$$v_{\mathrm{xc}\sigma}[|\varphi_{i\sigma}(\mathbf{r})|^2,0] = \left.\frac{\delta E_{\mathrm{xc}}[\{\varphi_{jv}[n]\}]}{\delta n_\sigma}\right|_{n=|\varphi_{i\sigma}|^2}. \tag{12}$$

The functional derivative can be evaluated using the optimized effective potential (OEP) formalism [60,103]. In the Supplemental Material to this paper [104], we demonstrate how to evaluate Eq. (11) for explicitly orbital-dependent functionals. In particular, for the OSIE of the global hybrid we find

$$\begin{aligned} e_{i\sigma}^{\mathrm{PBEh}}(a) = {} & (1-a)\langle\varphi_{i\sigma}|\big(v_{\mathrm{H}}[|\varphi_{i\sigma}|^2]+v_{\mathrm{x}\sigma}^{\mathrm{PBE}}[|\varphi_{i\sigma}|^2,0]\big)|\varphi_{i\sigma}\rangle \\ & + \langle\varphi_{i\sigma}|v_{\mathrm{c}\sigma}^{\mathrm{PBE}}[|\varphi_{i\sigma}|^2,0]|\varphi_{i\sigma}\rangle. \end{aligned} \tag{13}$$

Note that the OSIE of Eq. (13) depends on a in a structure similar to the xc energy in Eq. (4). This is consistent with the limiting cases: For $a=0$ the OSIE reduces to the one of pure PBE, while for $a=1$, i.e., full EXX with PBE correlation, the Hartree term as well as the PBE exchange are fully canceled, and only PBE correlation contributes to the OSIE.

For the local hybrids ISO and ISOII, on the other hand, it can be demonstrated that the Hartree term is completely canceled by the xc term in Eq. (11), since the latter reduces to pure EXX if evaluated on single spin-orbital densities only. Consequently, these functionals give an OSIE of zero independently of the parameter used, i.e.,

$$e_{i\sigma}^{\mathrm{ISO}}(c) = e_{i\sigma}^{\mathrm{ISOII}}(c^*) = 0 \quad \forall\, c,c^*. \tag{14}$$

The cancellation is triggered by the single spin-orbital detection functions $\tau_{\mathrm{W}}(\mathbf{r})/\tau(\mathbf{r})$ in the LMFs.

However, there is also a completely different approach to eliminate the one-error. Traditional SIC schemes [45,60] rely on Eq. (1) and define

$$E_{\mathrm{xc}}^{\mathrm{SIC}} = E_{\mathrm{xc}}^{\mathrm{approx}} - \sum_{i\sigma} \left\{ E_{\mathrm{H}}[n_{i\sigma}] + E_{\mathrm{xc}}^{\mathrm{approx}}[n_{i\sigma},0] \right\} \tag{15}$$

as the self-interaction corrected version of the approximate functional $E_{\mathrm{xc}}^{\mathrm{approx}}$.

It is important to note that Eq. (15) is not invariant under unitary transformations of the Kohn-Sham orbitals. Evaluation of Eq. (15) with orbitals that are transformed via $\tilde{\varphi}_{i\sigma}(\mathbf{r}) = \sum_{j=1}^{N_\sigma} U_{ij}^{\sigma}\, \varphi_{j\sigma}(\mathbf{r})$ results in an altered xc and, consequently, total energy, while leaving the electron density unchanged: $n(\mathbf{r}) = \sum_{i\sigma} |\varphi_{i\sigma}(\mathbf{r})|^2 = \sum_{i\sigma} |\tilde{\varphi}_{i\sigma}(\mathbf{r})|^2$. Kohn-Sham SIC schemes that incorporate a unitary transformation U_{ij}^{σ} into the OEP equation are referred to as generalized OEP SIC (GSIC) [40,47,105].

In the following, we discuss the consequences of removing the one-error (a) directly via a GSIC scheme, (b) nominally via the local hybrids ISO and ISOII and (c) partially via the global hybrid PBEh. For doing so we compare the corresponding Kohn-Sham eigenvalue spectra to experimental photoemission data for six prototypical organic molecules (see Fig. 1): the aromatic rings benzene, pyridine and pyrimidine, the polycyclic aromatic hydrocarbons pentacene and perylene as well as 1,4,5,8-naphthalene tetracarboxylic dianhydride (NTCDA), a model organic semiconductor. These systems are paradigm test cases for questions of treating SI and orbital localization with DFT.

In addition to the one-error we also examine the many-error. For this, we investigate the total energy curve as a function of particle number for the local hybrids ISO and ISOII as well as the global hybrid PBEh. We explicitly calculate the energy curves $E(N)$ for eight atoms and diatomic molecules between their neutral ($N_0 + 1$) and singly ionized state (N_0 electrons). In order to allow for a comprehensive evaluation of our results, we introduce (following Ref. [106]) the squared integrated many-electron SIE

$$\Xi = \sqrt{\int_{N_0}^{N_0+1} [(E(N) - E^{\mathrm{isl}}(N)]^2 \, \mathrm{d}N}. \tag{16}$$

Here, $E^{\mathrm{isl}}(N)$ denotes the straight line between adjacent integer particle numbers based on Eq. (2). It is obtained by linear interpolation between the calculated energy values at N_0 and $N_0 + 1$. The definition of Ξ was chosen such that Eq. (16) gives a measure of the many-error in energy units. Importantly, energy curves with both convex and concave parts are not falsely detected as obeying the straight-line criterion, since squaring the energy difference in Eq. (16) prevents an erroneous cancellation of terms under the integral. Instead, Ξ gives zero only for exact piecewise-linear behavior. Further, note that Eq. (2) provides a meaningful measure only for finite systems, as it has been demonstrated that the curvature of the energy curve naturally vanishes in the solid-state limit even for (semi)local density functionals [107].

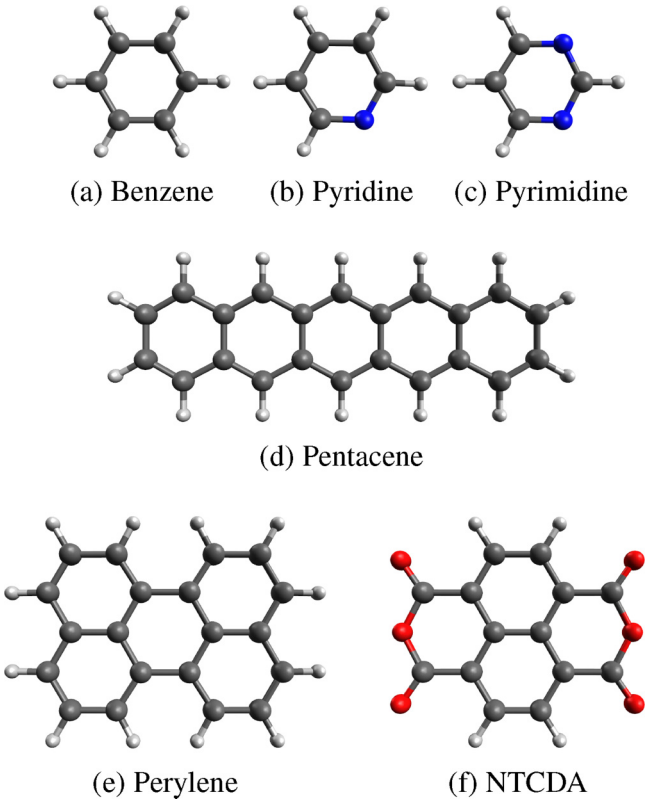

FIG. 1. Schematic illustration of the molecules studied in this paper. Carbon atoms are represented in black, hydrogen in white, nitrogen in blue, and oxygen in red.

IV. METHODOLOGY

The calculations of the $E(N)$ curves were carried out using the highly accurate real-space grid program DARSEC [88,108,109]. We calculate the energy curves for the atoms He, C, O, and Mg, as well as for the molecules BeH, CO, N_2, and NO. For the molecules, we use experimental bond lengths [110]. The integral in Eq. (16) is computed using the trapezoidal rule with a step size of $\Delta = 0.05$ for the fractional electron number N. Throughout this work, all orbital-dependent functionals are evaluated self-consistently by using the KLI approximation [111,112].

The systems in Fig. 1 are calculated using the Bayreuth version [31] of the program package PARSEC [113]. Core electrons are treated only implicitly via the pseudopotential (PP) approximation. Throughout this work, we employ consistent norm-conserving PPs of Troullier-Martins type [114] for (semi)local functionals. For orbital-dependent xc approximations such as hybrid functionals, constructing a consistent pseudopotential is very demanding [60]. We therefore here adopt a workaround strategy. For PBEh satisfying results for the Kohn-Sham eigenvalues can be obtained by employing

PBE or EXX [115] PPs (depending on a). We here use PBE PPs for the global hybrid with 25% EXX, while for higher fractions of EXX we use EXX PPs in combination with a Giannozzi-type PP for hydrogen [116] (see Appendix B for details regarding the PPs used in this paper).

For the local hybrids ISO and ISOII the question of a proper PP is yet more difficult. Using these functionals on top of PPs constructed with a different functional leads to eigenvalues that deviate noticeably from the ones of all-electron calculations. We explicitly checked this by comparing DARSEC and PARSEC results. However, there is a way to restore satisfying agreement in the Kohn-Sham eigenvalues for these functionals without having to go through the heavy work of constructing a truly consistent PP. The important step is to introduce a sort of "core-correction," based on the following idea: Since the crucial difference between global and local hybrids is the spatially resolved mixing of various functional ingredients, one must try to reproduce the all-electron structure of the LMFs of Eqs. (6), (7), (9), and (10) for ISO and ISOII, respectively, as close as possible in the PP calculation. In standard PP calculations, the xc energy and potential are obtained using only the valence density $n_\mathrm{v}(\mathbf{r})$. However, it is well understood that the core density $n_\mathrm{c}(\mathbf{r})$ around the atomic center has a large influence on detection functions such as $\tau_\mathrm{W}(\mathbf{r})/\tau(\mathbf{r})$ [117]. Therefore, it is important to explicitly include $n_\mathrm{c}(\mathbf{r})$ in the construction of the LMFs in order to correctly detect all spatial regions as intended in the construction of the xc energy density in Eq. (5).

For this, we replace the functions $\tau_\mathrm{W}(\mathbf{r})$, $\tau(\mathbf{r})$ and $t^2(\mathbf{r})$ in Eqs. (6), (7), (9), and (10) by their core-density (cd) corrected modifications

$$\tau_\mathrm{W}^\mathrm{cd}(\mathbf{r}) = \frac{|\nabla(n_\mathrm{v}(\mathbf{r})+n_\mathrm{c}(\mathbf{r}))|^2}{8(n_\mathrm{v}(\mathbf{r})+n_\mathrm{c}(\mathbf{r}))}, \tag{17}$$

$$\tau^\mathrm{cd}(\mathbf{r}) = \frac{1}{2}\left\{\left(\sum_{\substack{i\sigma\\ \text{valence}\\ \text{states}}} \left|\nabla\varphi_{i\sigma}^\mathrm{v}\right|^2\right) + \left|\nabla(n_\mathrm{c}(\mathbf{r}))^{\frac{1}{2}}\right|^2\right\}, \tag{18}$$

$$(t^\mathrm{cd}(\mathbf{r}))^2 = \left(\frac{\pi}{3}\right)^{1/3}\frac{a_0}{16\Phi^2(\zeta(\mathbf{r}))}\frac{|\nabla(n_\mathrm{v}(\mathbf{r})+n_\mathrm{c}(\mathbf{r}))|^2}{(n_\mathrm{v}(\mathbf{r})+n_\mathrm{c}(\mathbf{r}))^{7/3}}. \tag{19}$$

In our implementation the spin polarization only features the valence density, i.e., $\zeta(\mathbf{r}) = (n_{\mathrm{v}\uparrow}(\mathbf{r}) - n_{\mathrm{v}\downarrow}(\mathbf{r}))/(n_{\mathrm{v}\uparrow}(\mathbf{r}) + n_{\mathrm{v}\downarrow}(\mathbf{r}))$.

In Eq. (18) one identifies the second term on the RHS with the core contribution to the Kohn-Sham kinetic energy density, i.e.:

$$\sum_{\substack{k\nu\\ \text{core states}}} \left|\nabla\varphi_{k\nu}^\mathrm{c}(\mathbf{r})\right|^2 \approx \left|\nabla(n_\mathrm{c}(\mathbf{r}))^{\frac{1}{2}}\right|^2. \tag{20}$$

Equation (20) is exact for atoms with one (doubly occupied) core orbital of s character, since here $\varphi^\mathrm{c}(\mathbf{r}) = (n_\mathrm{c}(\mathbf{r}))^{\frac{1}{2}}$. Therefore, the organic molecules investigated in this publication are covered exactly, as they only consist of C, N, and O atoms in combination with H. For systems with more core orbitals (especially of p character), Eq. (20) would only be an approximation.

In the Supplemental Material [104] we compare the Kohn-Sham eigenvalues of ISO and ISOII obtained in PARSEC using EXX PPs to all-electron eigenvalues from DARSEC for the molecules NH, N_2, and CO. We find that the core-density corrected LMFs are crucial for reaching satisfying agreement with the all-electron results. Especially the higher lying valence states, on which we focus in Sec. V A, are described much more accurately by implicitly taking the core density into account.

In Ref. [89] it was demonstrated that the xc potential of local hybrids asymptotically decays with $v_{\mathrm{xc}\sigma} \to -\gamma_\sigma/|\mathbf{r}|$ for $|\mathbf{r}| \to \infty$ instead of the correct $-1/|\mathbf{r}|$ behavior [96,97]. Here,

$$\gamma_\sigma = 1 - \frac{1}{2}\int f_\mathrm{x}(\mathbf{r})|\varphi_{N_\sigma\sigma}|^2 \mathrm{d}^3r, \tag{21}$$

i.e., the asymptotical decay is not a global constant, but rather determined by the electronic structure of each system individually. The value of γ_σ offers a convenient way to compare the LMFs from the all-electron and the PP runs with and without the core-density correction in a single numerical value. Indeed we find that applying the core-density correction brings γ_σ in closer agrement with the all-electron calculations (see Ref. [104]).

In our GSIC calculations we use complex-valued energy-minimizing orbital transformations (labeled E-min GSIC). A local, multiplicative potential is obtained via the generalized OEP (GOEP) formalism. We here use the generalized KLI approximation (GKLI) [47] with the gradient-line-search algorithm for the energy-minimizing transformation as described in Ref. [105]. We apply the GSIC scheme of Eq. (15) to the LSDA, for the reasons given in Refs. [48,105], and use LSDA PPs as justified in Ref. [105].

V. RESULTS

A. Hybrid functionals and one-error: Simulated photoemission observables

In this section, we simulate photoemission spectra (PES) for the molecules of Fig. 1 by interpreting our calculated occupied Kohn-Sham eigenvalues as physical electron removal energies. For this, we align each eigenvalue spectrum to the first peak in the experimental gas phase photoemission spectrum and chose this as the zero of energy. Additionally, for evaluating the corresponding functional's performance with respect to the IP theorem, both the experimental IP and the (unshifted) negative ho eigenvalue are reported for each system. Further, we broaden the relative Kohn-Sham eigenvalue spectra by convolution with a Gaussian using a standard deviation of 0.08 eV in order to mimic the broadening of the experimental data. However, no uniform stretching [118] is applied to our computed spectra.

In order to discuss the connection between one-error and the interpretation of Kohn-Sham eigenvalues as a physical DOS, we here show the OSIE obtained by the global and local hybrids for the six organic molecules. For both ISO and ISOII we rely on the analytical argument of Eq. (14), i.e., a vanishing OSIE is obtained for all states independently of the functional parameter. The OSIE for PBEh is numerically evaluated using Eq. (13) after self-consistency is reached in the Kohn-Sham equations. In order to give a transparent overview over the

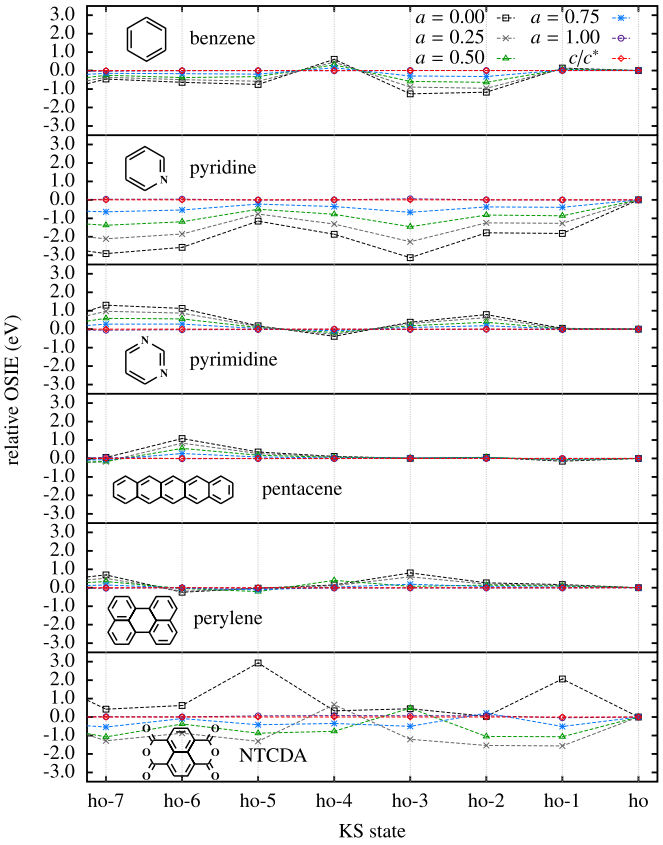

FIG. 2. Relative OSIE in eV for benzene, pyridine, pyrimidine, pentacene, perylene, and NTCDA. For PBEh the OSIE is numerically computed using Eq. (13) for different values of a. For the local hybrids ISO and ISOII the OSIE is zero according to Eq. (14).

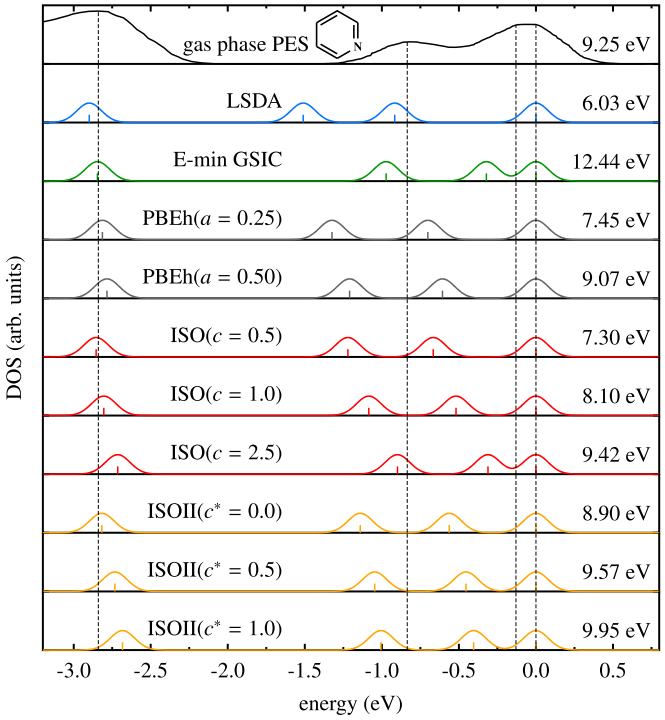

FIG. 3. Kohn-Sham DOS for pyridine obtained from different functionals compared to the experimental gas phase photoemission spectrum [119].

distortions introduced by SIE, the relative OSIEs $e_i - e_{\mathrm{ho}}$ are plotted in Fig. 2 by taking the OSIE of the ho Kohn-Sham state as reference.

We start our discussion with some general observations. For benzene, pyridine, pyrimidine, and NTCDA the OSIEs computed with pure PBE (black squares) show values that vary greatly from one state to another. Consequently, a large impact of the one-error on the Kohn-Sham DOS is to be expected in agreement with Refs. [32,100,102]. For pentacene and perylene, however, all higher valence states show almost the same OSIEs with respect to the ho state, resulting in a DOS that is expected to be much less distorted by SI [100].

Second, Fig. 2 shows that for all systems an increasing value of a in PBEh leads to smaller values of the relative OSIEs. For benzene, pyridine, pyrimidine, pentacene, and, except for the ho-4 and ho-3 state, also perylene, a higher amount of EXX has a "straightening" effect. For $a = 1.0$, i.e., using 100% EXX in combination with PBE correlation, the OSIEs are reduced to virtually zero for all systems, coinciding with the analytical results for the local hybrids. For NTCDA, this straightening effect also exists but is less obvious to discuss, as an increase in the amount of EXX leads to a change in both the OSIEs and the ordering of the Kohn-Sham orbitals, resulting in a more complicated curve.

Third, the OSIE curves obtained with PBEh($a = 0$), i.e., pure PBE exchange and correlation, are similar to the ones from other (semi)local functionals, as for example the LSDA. Therefore, it is justified to discuss the Kohn-Sham DOS of the LSDA in connection to the OSIEs of PBEh ($a = 0$).

Pyridine exhibits the strongest deviations in the relative OSIEs with values up to 3 eV for pure PBE. Indeed the Kohn-Sham DOS obtained from LSDA describes the experimental photo-emission spectrum insufficiently. Figure 3 shows that in the shifted spectrum especially the second and third peak are off by ≈0.5–1 eV, while also the ho eigenvalue of $-\varepsilon_{\mathrm{ho}} = 6.03$ eV drastically underestimates the experimental IP.

Explicit removal of the one-error leads to better agreement with the experimental spectrum, as the second and third eigenvalues obtained by E-min GSIC are shifted towards the corresponding experimental peaks. However, here the ho eigenvalue significantly overestimates the experimental IP. We attribute this to the "overcorrection" that can be seen in energy-minimizing SIC schemes, as discussed in Ref. [27]. The global hybrid PBEh moves the second and third eigenvalue towards the GSIC results when going from $a = 0.25$ to $a = 0.5$, as the one-error is increasingly compensated by the higher amount of EXX.

Interestingly, ISO and ISOII show Kohn-Sham eigenvalue spectra that are similar to the PBEh spectra. The fact that for global and local hybrids the description of the IP via $-\varepsilon_{\mathrm{ho}}$ depends decisively on the value of the respective functional parameter was investigated in detail in Refs. [56,88], finding a close connection with the incorrect asymptotical decay of $v_{\mathrm{xc}}(\mathbf{r})$ for both types of hybrids [89].

Also the occupied Kohn-Sham eigenvalues below the ho state show striking similarities for the global and local hybrids. Here, the agreement with physical removal energies improves

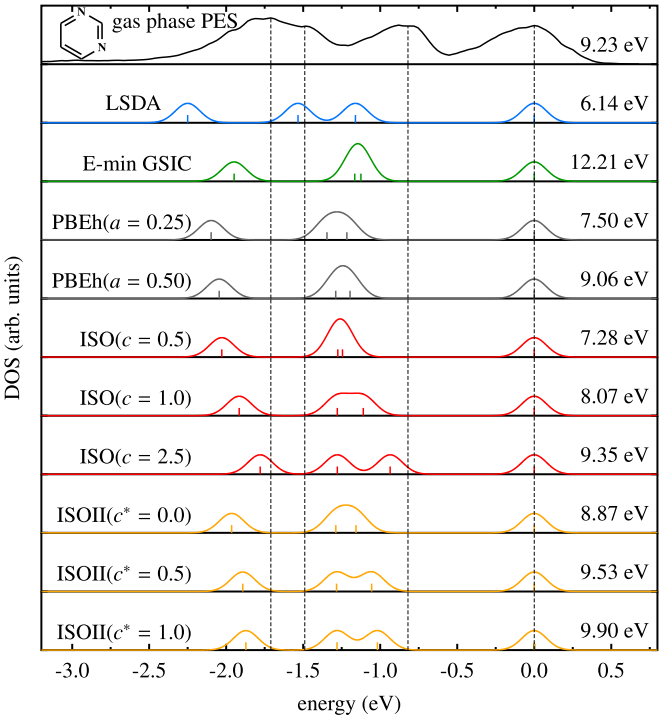

FIG. 4. Kohn-Sham DOS for pyrimidine obtained from different functionals compared to the experimental gas phase photoemission spectrum [120].

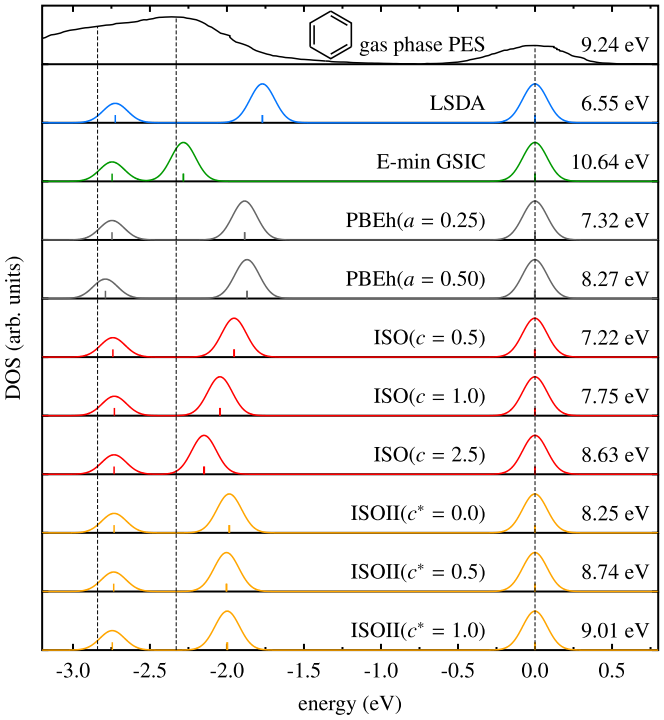

FIG. 5. Kohn-Sham DOS for benzene obtained from different functionals compared to the experimental gas phase photoemission spectrum [119].

if the value of the corresponding functional parameter is increased. Especially the Kohn-Sham eigenvalues of the ho-2 and ho-3 state are moved towards the experimental peaks, similar to the ones of PBEh. From the perspective that the local hybrids are nominally free from one-error with systematically vanishing OSIEs, one would intuitively expect a spectrum closer to the one obtained by GSIC. Our results show that it is in principle possible to obtain a DOS comparable to GSIC with ISO and ISOII using relatively large parameters. However, the eigenvalues of GSIC and the local hybrids do not describe physical energies with the same accuracy *independent of the value of the functional parameter*, as their systematically vanishing OSIE might suggest. Consequently, the fact that the interpretability of Kohn-Sham eigenvalues as physical energies for these functionals depends on the amount of EXX rather than on the property of being free from one-error demonstrates a fundamental point: the OSIE is a necessary, but not sufficient criterion for judging the quality with which Kohn-Sham eigenvalues approximate physical electron removal energies.

The calculated eigenvalues of pyrimidine depicted in Fig. 4 confirm these statements. Here, increasing the functional parameter of the local hybrids has a large impact on the relative position of the ho-1 and ho-3 orbital, shifting them towards physically meaningful energies. However, the DOS of ISO and ISOII for large values of their parameter deviates from the GSIC spectrum. While GSIC predicts the ho-1 and ho-2 state to be nearly degenerate, the local hybrid functionals open up a gap between these eigenvalues and shift the ho-1 towards the corresponding experimental peak. Using such a parametrization, the local hybrids therefore even outperform GSIC for this system, while at the same time delivering a more realistic prediction of the IP via the ho eigenvalue.

The results for benzene in Fig. 5 underline how the relative OSIEs predict the problem of describing the experimental photoemission spectrum via the LSDA. Removing the one-error via GSIC significantly opens up the gap between the twofold degenerate ho and ho-1 and the ho-2 and ho-3 states.

Interestingly, both PBEh and ISOII show a reduced dependency on their functional parameter for the position of the ho-2 and ho-3 states. The local hybrid ISO on the other hand moves these states towards the experimental peak and the GSIC results. For values of $c \gtrsim 2.5$ ISO offers the possibility to describe the photoemission spectrum of benzene with an accuracy comparable to GSIC, while again it remedies the overestimation of the IP using $-\varepsilon_{\mathrm{ho}}$.

As discussed earlier in this section, the molecules pentacene and perylene show only small differences in the relative OSIEs for the valence states. Indeed Figs. 6 and 7 show that the (shifted) LSDA eigenvalues describe the experimental spectrum reasonably well. Furthermore, removing the one-error explicitly via GSIC has almost no effect on the Kohn-Sham DOS, but only results in a uniform shift on the spectrum, as the corresponding eigenvalue of the ho state indicates.

Similarly, an increase in the amount of EXX has no considerable effect on the Kohn-Sham DOS of the global and local hybrids. Figures 6 and 7 depict the simulated spectra using PBEh ($a = 0.25$), ISO ($c = 0.5$) and ISOII ($c^* = 0$). The spectra using larger values for the corresponding parameter look very similar (see Supplemental Material [104] for all spectra).

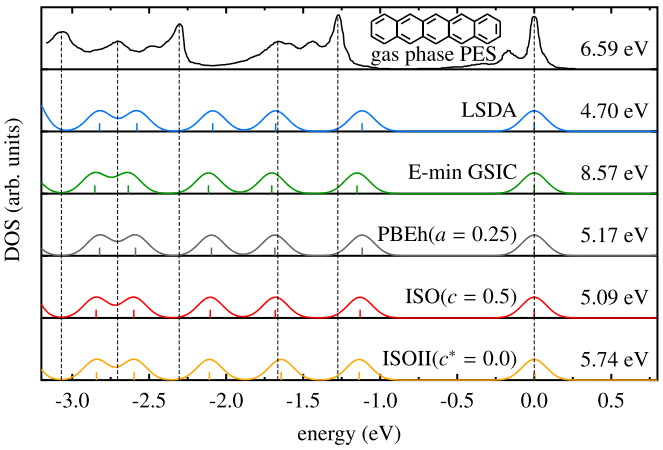

FIG. 6. Kohn-Sham DOS for pentacene obtained from different functionals compared to the experimental gas phase photoemission spectrum [121].

Our findings confirm that for systems for which the OSIEs of (semi)local functionals suggest negligible distortions in the Kohn-Sham eigenvalue spectrum, any additional mechanism to counteract one-error has no considerable effect on the aligned spectrum. This was demonstrated in Ref. [100] for global hybrid functionals and is here confirmed for local hybrids and GSIC. Note that in such cases as, e.g., pentacene and perylene, both local and global hybrids offer a more satisfying description of the photoemission spectrum, because when their respective functional parameter is chosen large enough, the agreement between the experimental IP and $-\varepsilon_{\mathrm{ho}}$ improves [122].

Figure 8 shows the comparison of Kohn-Sham eigenvalues to the experimental spectrum for NTCDA. Here, especially the position of the ho-1 state suffers from one-error, as its OSIEs in Fig. 2 suggest. Consequently, the LSDA predicts a DOS with a too narrow gap between the ho and ho-1 state. Applying the GSIC to this system opens up this gap drastically and shows eigenvalues that can better be interpreted as physical ionization energies.

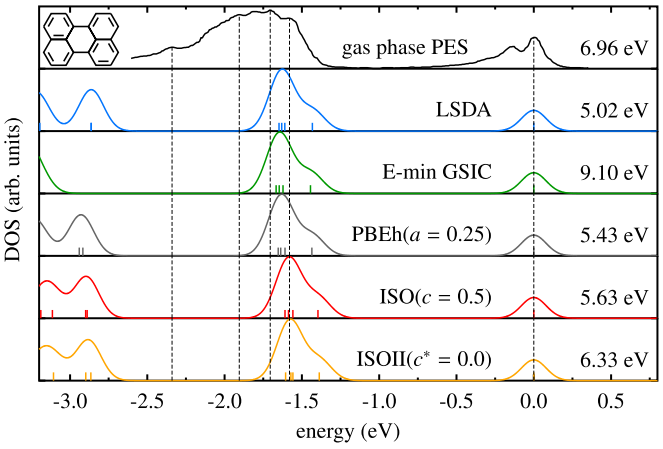

FIG. 7. Kohn-Sham DOS for perylene obtained from different functionals compared to the experimental gas phase photoemission spectrum [121].

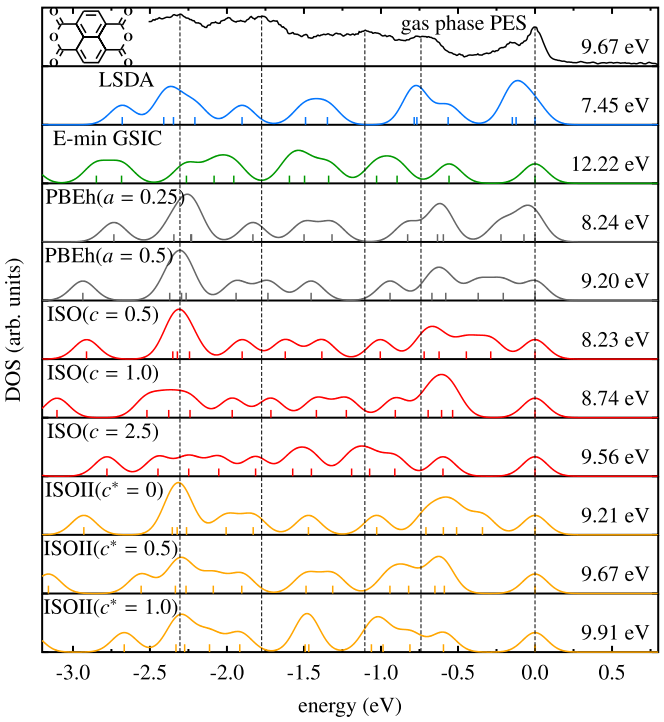

FIG. 8. Kohn-Sham DOS for NTCDA obtained from different functionals compared to the experimental gas phase photoemission spectrum [123].

For this system, all hybrid functionals shift the ho-1 eigenvalue towards the experimental energy if the value of the respective parameter is increased. Here, it is worth to discuss the performance of ISO using $c = 0.5$ in contrast to PBEh with $a = 0.25$. In these respective parametrizations, both functionals show their best performance for thermochemical properties [88,90]. However, the corresponding Kohn-Sham DOS in Fig. 8 demonstrates that ISO($c = 0.5$) delivers eigenvalues of a higher interpretability, as it noticeably opens the gap between the ho and ho-1 state when compared to PBEh ($a = 0.25$).

The hybrid functionals offer the possibility to reproduce the Kohn-Sham eigenvalue structure of GSIC, requiring large values of the respective functional parameter. On the one hand such a choice enhances the description of the overall IP via $-\varepsilon_{\mathrm{ho}}$ and remedies the systematical overestimation of this quantity in GSIC. Yet, it conflicts with the performance of hybrid functionals for other ground-state properties. Importantly, the ISO and ISOII spectra agree acceptably well with the E-min GSIC result only for large values of c and c^*. This underlines the finding that a nominal freedom from one-error does not universally guarantee the same quality of results compared to a direct removal of the SIE in the sense of Eq. (15). Instead, in analogy to global hybrids, the amount of EXX plays the dominant role for the interpretability of Kohn-Sham eigenvalues.

It has been demonstrated that SI not only affects the quality of Kohn-Sham eigenvalues, but also hinders the interpretation of intensity patterns observed in angular-resolved photoemission spectroscopy (ARPES) [32,33,35,36,124,125]. Based on the assumption that during the emission process the electron

method	ordering
ARPES map [35]	**A - B**
E-min GSIC	**A - B**
LSDA	C - A
PBEh($a = 0.00$)	C - A
PBEh($a = 0.25$)	A - C
PBEh($a = 0.50$)	A - C
PBEh($a = 0.75$)	A - C
PBEh($a = 1.00$)	**A - B**
ISO($c = 0.0$)	C - A
ISO($c = 0.2$)	A - C
ISO($c = 0.5$)	A - C
ISO($c = 1.0$)	A - C
ISO($c = 1.5$)	**A - B**
ISO($c = 2.0$)	**A - B**
ISO($c = 2.5$)	**A - B**
ISOII($c^* = 0.0$)	A - C
ISOII($c^* = 0.5$)	**A - B**
ISOII($c^* = 1.0$)	**A - B**
ISOII($c^* = 1.5$)	**A - B**

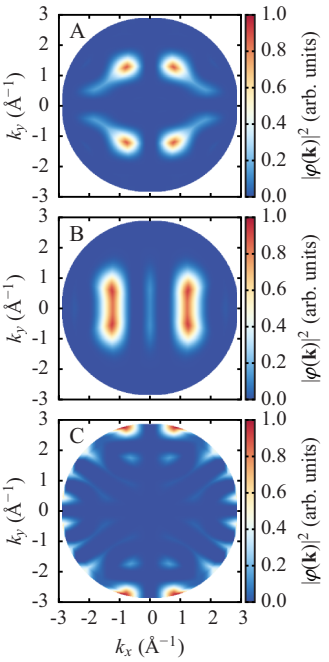

FIG. 9. Left side: Orbital ordering of the ho and ho-1 state for NTCDA calculated with different functionals in comparison to the ordering obtained in ARPES experiments. Agreement with experiment is marked in boldface. Right side: ARPES momentum maps of three NTCDA Kohn-Sham orbitals at $|\mathbf{k}| = 2.75$ Å^{-1}.

performs a transition from one particular molecular orbital to a plane-wave final state (see details in Refs. [126,127]), the photoemission intensity can be expressed as

$$I(k_x, k_y, E_{\text{kin}}) \propto |\varphi_{i\sigma}(\mathbf{k})|^2_{|\mathbf{k}|=\text{const.}}. \tag{22}$$

Equation (22) directly relates the emission intensity measured in ARPES experiments to the Fourier transform of a molecular orbital $|\varphi_{i\sigma}(\mathbf{k})|^2$, with $|\mathbf{k}|$ denoting the momentum of the outgoing electron. In order to discuss the relation between one-error and the interpretation of higher lying Kohn-Sham orbitals as ARPES momentum maps, we present two-dimensional representations of the corresponding fourier-transformed orbitals for the NTCDA molecule. Due to energy conservation and the relation $E_{\text{kin}} = |\mathbf{k}|^2/2$, $|\varphi_{i\sigma}(\mathbf{k})|^2$ has to be evaluated on a sphere with radius $|\mathbf{k}|$. This translates into a spherical cut through the three-dimensional orbital in $\mathbf{k}$-space, as it is shown in color code in the following. For our discussion we make use of the finding that for the molecule and momentum range studied here, the Kohn-Sham orbitals obtained with different functionals are in most cases quite similar and therefore result in quite similar momentum maps. In other words, we here focus on the relative ordering of the states.

Figure 9 shows the plots for the relevant transformed π (A and B) and σ orbitals (C) as a function of k_x and k_y, evaluated at a fixed kinetic energy. Experimentally confirmed by ARPES are the momentum maps A and B of the two π orbitals, with A having the smaller binding energy. Therefore, map A can be identified with the ho and B with the ho-1 state of the NTCDA molecule. Purely (semi)local functionals such as the LSDA and PBE do not reproduce this ordering, as they predict the ho state to be of type C, originating from a σ orbital not observed in ARPES experiments among the first two peaks. PBEh interchanges the ordering of the ho and ho-1 Kohn-Sham orbitals for intermediate values of the parameter a, while the correct ordering A–B is only reproduced for large amounts of EXX. Explicit removal of the one-error via GSIC gives the experimentally observed orbital ordering [35].

For ISO, a picture in analogy to PBEh occurs. ISO($c = 0$) reduces to pure LSDA for spin-unpolarized systems, and it consequently predicts a momentum map of type C for the ho state. Increasing the amount of EXX puts the map of type A in the first position, while incorrectly predicting the ho-1 state to be of type C. The correct ordering of momentum maps for both the ho and ho-1 state is only reproduced for large values of the functional parameter. The same mechanism emerges for ISOII, even though here the amount of EXX introduced via the modified LMF in Eq. (9) is intrinsically larger, resulting in the orbital ordering A–C for $c^* = 0$, while higher values of this parameter lead to the correct ordering.

These results again support the conclusion that the local hybrid functionals, despite being nominally free from one-error, reliably predict photoemission observables only for sufficiently large values of their respective functional parameter. We conclude that counteracting the one-error via spatially resolved single-orbital detection functions does not guarantee that Kohn-Sham eigenvalues and orbitals are as close to the physical quantities as the eigenvalues and orbitals that are found when the one-error is removed based on Eq. (15).

B. Hybrid functionals and many-error: Energy curves for fractional charges

In the previous subsection we discussed that global and local hybrids formally treat the one-error very differently, yet show a similar performance for quantities influenced by one-error. Naturally, the question arises whether the nominal freedom from one-error of local hybrids influences the many-error. In Ref. [106], $E(N)$ was discussed in detail for several local hybrids, focusing on the influence of range-separated components in the hybrid construction. In this paper, we concentrate on the question of how the conceptual freedom from one-error in a local hybrid functional affects the energy curves.

In this discussion we restrict ourselves to the different types of hybrid functionals and leave out SIC schemes based on Eq. (15). This has two reasons. First, an interesting SIC scheme employing fractional particle numbers has been put forward [15]. Yet, as it is based on off-diagonal Lagrangian multipliers [128] it goes beyond the Kohn-Sham concept of DFT on which we focus in this paper. Second, the previously discussed Kohn-Sham GSIC [40,47,105] requires a unitary orbital transformation which we so far could not extend to fractional particle numbers.

Therefore, we explicitly evaluate total energy curves $E(N)$ for the global and local hybrids and compare our calculated curves to the expected piecewise linear behavior, Eq. (2). We here focus on systems with particle numbers between their neutral and singly ionized state, i.e., $N = N_0 + \omega$ with $N_0 \in \mathbb{N}$

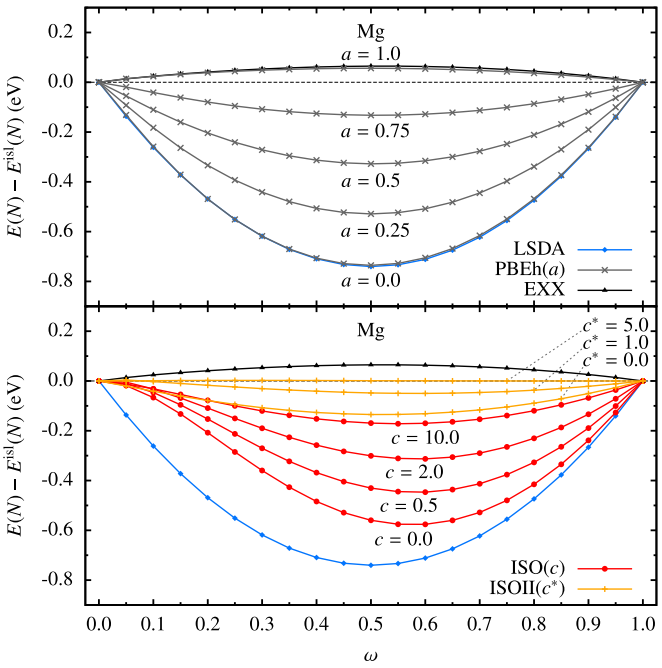

FIG. 10. $E(N) - E^{\mathrm{isl}}(N)$ as a function of the fractional electron number $N = N_0 + \omega$ for the magnesium atom. The curves were obtained using the LSDA, pure EXX and the global hybrid PBEh (upper panel) as well as the local hybrids ISO and ISOII (lower panel) for different values of the respective functional parameter. The piecewise-linear result is indicated by the dashed line.

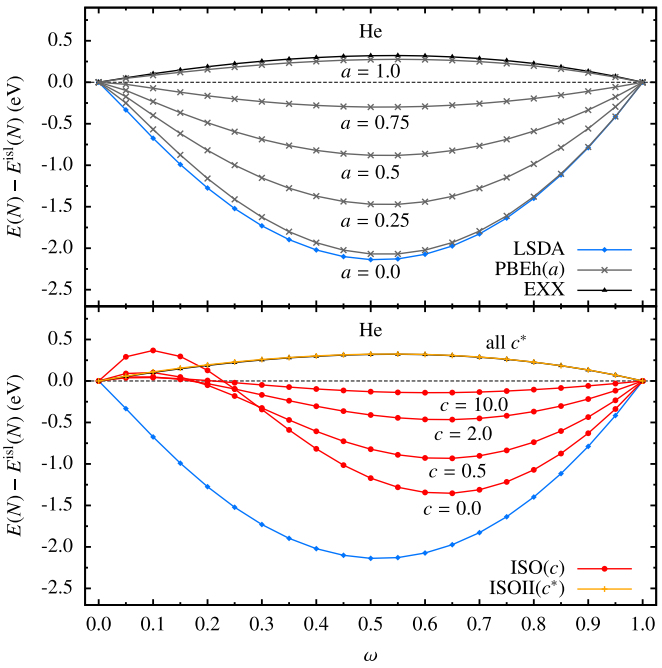

FIG. 11. $E(N) - E^{\mathrm{isl}}(N)$ as a function of the fractional electron number $N = N_0 + \omega$ for the helium atom. The curves were obtained using the LSDA, pure EXX and the global hybrid PBEh (upper panel) as well as the local hybrids ISO and ISOII (lower panel) for different values of the respective functional parameter. The piecewise-linear result is indicated by the dashed line.

and $w \in [0,1[$. Instead of plotting the calculated energy curves directly, it is beneficial to illustrate the difference $E(N) - E^{\mathrm{isl}}(N)$.

Figure 10 shows these curves for the magnesium atom. We clearly see the concave behavior found for pure EXX, and the convex deviation from piecewise linearity observed for the LSDA and PBE. Naturally, for global hybrid functionals one expects that there exists a certain mixing ratio of nonlocal and (semi)local components that minimizes the deviation from the straight-line behavior [92]. Figure 10 indeed demonstrates that an increasing amount of EXX in PBEh reduces the convexity until it is (almost) fully canceled and turned to concavity for large values of a.

For local hybrid functionals, due to their approach of flexible instead of rigid mixing, it is less clear what energy curve to expect. We find that the ISO functional also shows curves with reduced convexity for increasing values of c. However, in contrast to the results of LSDA, PBEh and EXX calculations, the local hybrid curves are noticeably asymmetrical. This asymmetry is introduced by the sensitivity of the LMF [Eq. (6)] to the electronic structure of the underlying system. Especially the explicit occurrence of the spin polarization in the LMF leads to an asymmetry in $E(N)$, as can be explained on the example of ISO using $c = 0$: The neutral magnesium atom has $\zeta(\mathbf{r}) = 0$, reducing ISO($c = 0$) to the LSDA since in this case $f_{\mathrm{x}}(\mathbf{r}) = f_{\mathrm{c}}(\mathbf{r}) = 1$. Consequently, for $\omega \to 1$ the energy curves of ISO($c = 0$) and LSDA agree well. Towards $\omega \to 0$ a finite spin-polarization $\zeta(\mathbf{r}) \neq 0$ is built up due to the fractional electron missing, resulting in $f_{\mathrm{x}}(\mathbf{r}) < 1$ and a partial inclusion of EXX. Therefore, the energy curve is shifted upwards, leading to the observed asymmetry. Note that not only $\zeta(\mathbf{r})$, but also the other functional ingredients $\tau_{\mathrm{W}}(\mathbf{r})/\tau(\mathbf{r})$ and $t^2(\mathbf{r})$ contribute to the asymmetry in $E(N)$. Thus, a similar effect is observed for the energy curves obtained with ISOII, though with smaller magnitude.

In the case of the helium atom, this effect leads to an interesting feature in the energy curves. Figure 11 shows rather symmetrical energy curves for the LSDA, EXX, and PBEh. ISO, on the other hand, gives curves with both convex and concave parts, i.e., $E(N)$ shows an inflection point and an intersection with the piecewise linear curve for $\omega \neq 0,1$. This peculiarity can also be explained with the example of ISO($c = 0$). While for $\omega \to 1$ the functional reduces to the LSDA, the singly ionized helium atom at $\omega \to 0$ only has one remaining electron, for which ISO reduces to pure EXX. Consequently, varying ω from 0 to 1 changes the functionals character from fully nonlocal to purely local, resulting in the observed curves.

An increase in the functional parameter c smoothens the curves and reduces the deviation from piecewise linearity. The energy curves obtained via ISOII for the helium atom coincide with the results of a pure EXX computation independently of c^*, due to the fact that setting $\zeta = 1$ leads to vanishing LMFs in Eq. (9) and (10) for a density built up of two identical Kohn-Sham orbitals of opposite spin.

Connected to this qualitative discussion of exemplary energy curves, we present a quantitative analysis of the deviation from piecewise linearity for the hybrids, using LSDA and EXX results as references values. For this, we rely on Ξ as introduced in Eq. (16). The corresponding results are presented

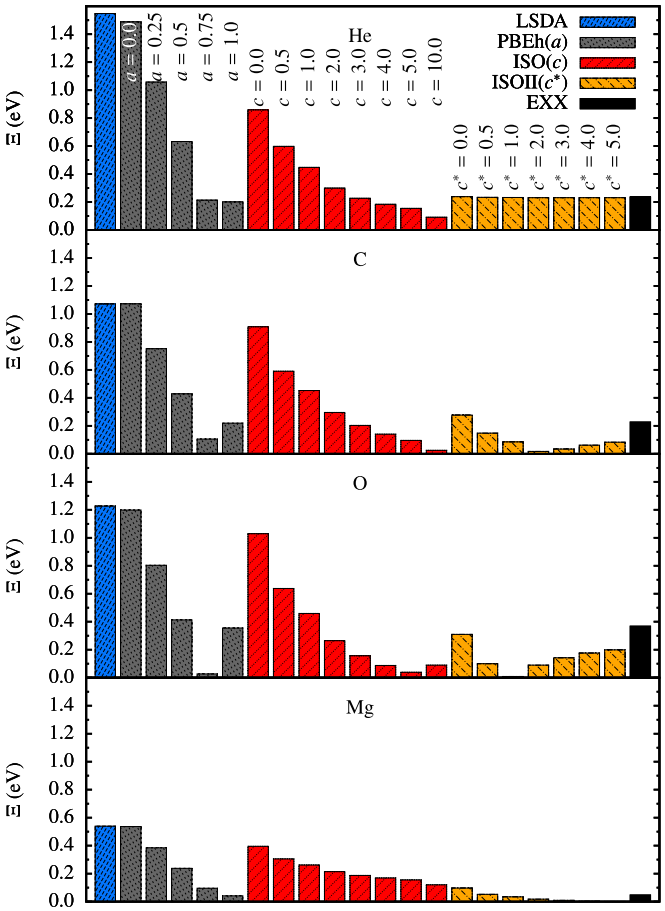

FIG. 12. Ξ [Eq. (16)] in eV for the atoms helium, carbon, oxygen and magnesium obtained using the LSDA, EXX, PBEh, ISO, and ISOII.

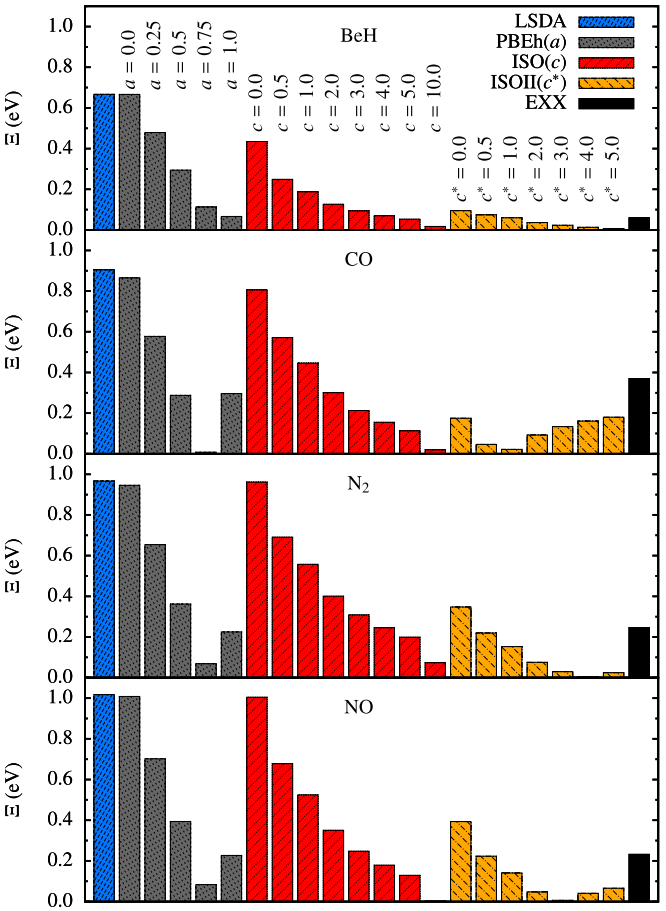

FIG. 13. Ξ [Eq. (16)] in eV for the molecules BeH, CO, N_2, and NO obtained using the LSDA, EXX, PBEh, ISO, and ISOII.

for the atoms He, C, O, and Mg in Fig. 12 and the molecules BeH, CO, N_2, and NO in Fig. 13. These system were chosen as they represent a small, transparent set of atoms and molecules which yet is diverse enough to lead to different electronic configurations in their ground and singly ionized states.

The LSDA and PBE perform similarly, being the functionals that deviate the most from piecewise linearity for almost all systems investigated. Interestingly, the magnesium atom in general shows small deviations with $\Xi = 0.54$ eV for the LSDA in contrast to, e.g., helium with $\Xi = 1.55$ eV. Pure EXX reduces Ξ considerably for all systems when comparing to (semi)local functionals, and the remaining error always originates from concavity. As already indicated for magnesium and helium, PBEh with a large fraction of EXX can nearly restore piecewise linearity by mixing convex (semi)local with concave functional components. As a result, most of the atoms and molecules in Figs. 12 and 13 show a minimum in Ξ around $a \approx 0.75$. This finding supports the connection between piecewise linearity and the description of IPs via $-\varepsilon_{\mathrm{ho}}$, since PBEh was found to perform best in the latter category using this parametrization as well [56].

The local hybrid ISO evaluated with $c = 0$ already reduces Ξ in comparison with the (semi)local LSDA and PBE especially for the atoms and the BeH molecule. For these systems, we further observed that ISO($c = 0.5$) outperforms the comparable global hybrid PBEh($a = 0.25$), meaning that it reduces the many-error while performing similar for quantities related to thermochemistry. The reduction of Ξ for ISO in contrast to the comparably parametrized global hybrid is mostly due to the explicit inclusion of $\zeta(\mathbf{r})$ in the functional construction and the consequences for piecewise linearity described in detail above. For the molecules CO, N_2, and NO this effect appears less pronounced, as here the removal of one electron has a smaller impact on the spin polarization.

Apart from these features, both ISO and PBEh display a similar dependence of Ξ on their respective functional parameter. Our calculations show that the local and global hybrid systematically reduce Ξ when the amount of EXX is increased. ISO minimizes Ξ for values between $c \approx 5$–10 for the systems C, CO, NO, O, while the other molecules and atoms require even larger values of the functional parameter to considerably reduce the deviation from piecewise linearity in their energy curves. Again, this result agrees with the finding that describing IPs via the ho Kohn-Sham eigenvalue using this local hybrid functional requires a similar parametrization [88].

Our results support the conclusion that the formal criterion of a functional being free from one-error does not guarantee a good performance with respect to the energy curves $E(N)$, a manifestation of the many-error. This finding is in line with the results of Ref. [58]. Thus, we arrive at the same principle

discussed in Sec. V A for the influence on the one-error: For both local and global hybrids, the amount of EXX included plays the decisive role regarding the performance for properties dominated by the many-error. In that sense, global and local hybrids can be thought of as two sides of the same medal.

This finding is further supported by evaluating Ξ for ISOII in Figs. 12 and 13. Setting $\zeta(\mathbf{r}) = 1$ in its LMFs in Eqs. (9) and (10) systematically reduces the values that these functions take, resulting in instrically higher portions of EXX. Consequently, ISOII shows the smallest deviations from piecewise linearity. Especially the energy curve for the magnesium atom in Fig. 10 shows how this local hybrid restores the correct total energy dependency on fractional charges for large values of the functional parameter c^*. However, also here the performance with respect to many-error depends strongly on the functional's parameter, and in this sense ISOII can be understood as a continuation of ISO with larger functional parameter.

VI. CONCLUSIONS

In this work we shed light on the manifestation of the one- and many-electron self-interaction error in global and local hybrid functionals. Our first focus was on investigating whether local hybrids that are formally one-electron self-interaction free are superior to global hybrids with respect to the interpretation of their Kohn-Sham eigenvalues and orbitals as photoemission observables. To this end, we also compared the iso-orbital indicator $(\tau_W(\mathbf{r})/\tau(\mathbf{r}))$ based self-interaction correction of the local hybrids to the GSIC, i.e., a Perdew-Zunger type Kohn-Sham self-interaction correction. We found that compared to LSDA and a GGA, the local hybrid functionals can considerably increase the interpretability of Kohn-Sham eigenvalues as electron removal energies, similar to GSIC. However, the local hybrids' performance depends very much on the value of a parameter that appears in these functionals. Large values for the parameter, corresponding to a large exact exchange component, are necessary to obtain physically meaningful eigenvalues. In this sense, local hybrids are much like global hybrids. With a properly chosen parameter, hybrid functionals lead to highest occupied eigenvalues that approximate experimental IPs better than GSIC eigenvalues.

In a second step we discussed the total energy as a function of particle number for local and global hybrids. For the smaller systems in our study we found that a local hybrid can lead to a reduction of many-electron self-interaction in comparison to a global hybrid due to the mixing function's sensitivity on the systems' spin polarization. The latter changes naturally upon addition or removal of an electron. For larger systems, however, removal of one electron only causes a relatively small change in the spin densities, and the local hybrid again becomes more similar to a global hybrid. A similarity between local and global hybrids also emerges for the electron-transfer characteristics in hydrogen chains that we discuss in Appendix A.

Our findings demonstrate that there is a conceptual difference between the different ways of how the one-electron condition Eq. (1) is used in a many-electron system. While Eq. (1) poses a stringent test for functionals in the one-electron case, it does not provide a unique construction rule for density functionals, and obeying Eq. (1) does not guarantee reliable results for many-electron systems. In particular, under different perspectives we arrive at the conclusions that although local hybrids can be formally made one-electron self-interaction free with the help of detection functions such as $\tau_W(\mathbf{r})/\tau(\mathbf{r})$, this does not necessarily remove self-interaction in the same way as the Perdew-Zunger concept of Eq. (15). Thus, local hybrid functionals based on the concept of canceling self-interaction with the help of semilocal detection functions appear as elaborate extensions of global hybrids, sharing some of their basic shortcomings, while offering some additional benefits through the flexible mixing of non and semilocal functional components.

ACKNOWLEDGMENTS

We acknowledge the support of and fruitful discussions with Matthias Dauth regarding the interpretation of Kohn-Sham orbitals as ARPES maps. We are gratefuly to Eli Kraisler and Leeor Kronik for many fruitful discussions about hybrid functionals in general. Financial support by the German-Israeli Foundation is gratefully acknowledged.

APPENDIX A: ELECTRON TRANSPORT IN HYDROGEN CHAINS

We here investigate the charge transfer (CT) properties of a model system consisting of two hydrogen chains, each containing eight hydrogen atoms separated by 1 Å. These chains are aligned along the x axis, located at a distance of 8 Å as illustrated in the inset of Fig. 14. We then switch on a constant electric field in the x direction, which induces CT from the right (donor) to the left (acceptor) hydrogen chain. In order to quantize the simulated CT from the donor to the acceptor chain, we investigate the charge density integrated in the acceptor's semisphere as a function of the applied field strength. Figure 14 shows the results obtained using the LSDA, E-min GSIC, and ISO with $c = 0.5$ and $c = 5.0$. Note that for some values of the electric field no convergence could be reached for ISO, since the calculation repeatedly jumped between different solutions.

Due to their large separation and small coupling, CT between the hydrogen chains must occur via integer electron jumps at certain field strengths [42,44]. However, the LSDA gives a qualitatively wrong picture of the CT: Beginning at a field strength of $\approx 2.0 \times 10^9 \frac{\mathrm{V}}{\mathrm{m}}$, fractional charges are

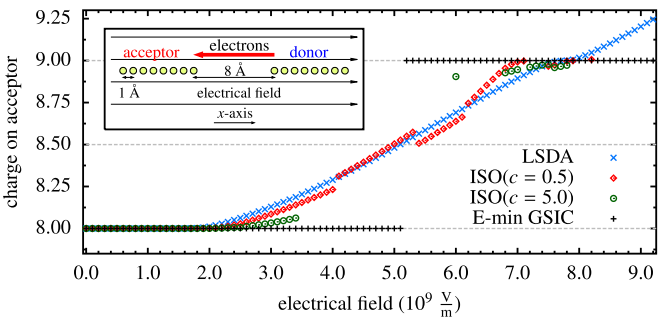

FIG. 14. Integrated charge density on the acceptor in dependence on the strength of the external electrical field.

gradually transferred from the donor to the acceptor chain. At $\approx 7.8 \times 10^9 \frac{\mathrm{V}}{\mathrm{m}}$ one whole electron has migrated, while higher field values again induce fractional CT. In contrast, removal of the one-error via GSIC results in the physical integer electron transfer, occurring at a field strength of $\approx 5.1 \times 10^9 \frac{\mathrm{V}}{\mathrm{m}}$ [129].

We now investigate the performance of a nominally one-error free local hybrid functional. Figure 14 shows that using ISO with a parameter of $c = 0.5$ slightly improves over the LSDA curve by shifting the appearance of fractional CT towards higher field strengths, while at the same time broadening the plateau around ≈ 7–$8 \times 10^9 \frac{\mathrm{V}}{\mathrm{m}}$. Increasing the functional parameter to $c = 5.0$ further improves the simulated CT properties, as here fractional charge transfer sets in at even higher field strengths.

It thus becomes apparent that the performance of the local hybrid decisively depends on the amount of EXX included, a feature that is also observed for global hybrids [42]. Consequently, the CT studied here is another example for the similarity between local and global hybrids functionals.

APPENDIX B: PSEUDOPOTENTIALS DETAILS

We here specify all details regarding the PPs used throughout this work. Table I lists which functional is used with which PP. For each atom the corresponding cutoff radii are given in bohrs. For the local hybrid functionals, the explicit use of the core densities as explained in Sec. IV is marked by the note "with n_c."

TABLE I. Specifications of the PPs. DF denotes the density functional.

DF	DF PP	atom	$r_c(s)$	$r_c(p)$
LSDA, E-min GSIC	LSDA	H	1.39	
		C	1.60	1.60
		N	1.50	1.50
		O	1.45	1.45
PBE, PBEh ($a = 0.25$)	PBE	H	1.40	
		C	1.49	1.53
		N	1.50	1.50
		O	1.45	1.45
PBEh ($a \geqslant 0.50$)	Giannozzi	H		
	EXX	C	1.20	1.20
		N	1.19	1.19
		O	0.99	0.94
ISO (c)	Giannozzi	H		
ISOII (c^*)	EXX	C	1.20	1.20
	with n_c	N	1.19	1.19
		O	0.99	0.94

[1] P. Hohenberg and W. Kohn, Phys. Rev. **136**, B864 (1964).
[2] W. Kohn and L. Sham, Phys. Rev. **140**, A1133 (1965).
[3] R. G. Parr and W. Yang, *Density-Functional Theory of Atoms and Molecules* (Oxford University Press, New York, 1989).
[4] C. Fiolhais, F. Nogueira, and M. Marques, editors, *A Primer in Density Functional Theory* (Springer-Verlag, Berlin-Heidelberg, 2003).
[5] R. O. Jones, Rev. Mod. Phys. **87**, 897 (2015).
[6] K. Burke, J. Chem. Phys. **136**, 150901 (2012).
[7] D. Ceperley and B. Alder, Phys. Rev. Lett. **45**, 566 (1980).
[8] S. H. Vosko, L. Wilk, and M. Nusair, Can. J. Phys. **58**, 1200 (1980).
[9] J. P. Perdew and Y. Wang, Phys. Rev. B **45**, 13244 (1992).
[10] J. P. Perdew, K. Burke, and M. Ernzerhof, Phys. Rev. Lett. **77**, 3865 (1996).
[11] J. P. Perdew, K. Burke, and M. Ernzerhof, Phys. Rev. Lett. **78**, 1396 (1997).
[12] T. Bally and G. N. Sastry, J. Phys. Chem. A **101**, 7923 (1997).
[13] Y. Zhang and W. Yang, J. Chem. Phys. **109**, 2604 (1998).
[14] P. Mori-Sánchez, A. J. Cohen, and W. Yang, J. Chem. Phys. **125**, 201102 (2006).
[15] O. A. Vydrov, G. E. Scuseria, and J. P. Perdew, J. Chem. Phys. **126**, 154109 (2007).
[16] J. P. Perdew, Adv. Quantum Chem. **21**, 113 (1990).
[17] A. Ruzsinszky, J. P. Perdew, G. I. Csonka, O. A. Vydrov, and G. E. Scuseria, J. Chem. Phys. **125**, 194112 (2006).
[18] A. D. Dutoi and M. Head-Gordon, Chem. Phys. Lett. **422**, 230 (2006).
[19] O. V. Gritsenko and E. J. Baerends, Int. J. Quantum Chem. **106**, 3167 (2006).
[20] J. P. Perdew, A. Ruzsinszky, G. I. Csonka, O. A. Vydrov, G. E. Scuseria, V. N. Staroverov, and J. Tao, Phys. Rev. A **76**, 040501 (2007).
[21] A. Makmal, S. Kümmel, and L. Kronik, Phys. Rev. A **83**, 062512 (2011).
[22] B. Champagne, E. A. Perpete, S. J. A. van Gisbergen, E. J. Baerends, J. G. Snijders, C. Soubra-Ghaoui, K. A. Robins, and B. Kirtman, J. Chem. Phys. **109**, 10489 (1998).
[23] S. J. A. van Gisbergen, P. R. T. Schipper, O. V. Gritsenko, E. J. Baerends, J. G. Snijders, B. Champagne, and B. Kirtman, Phys. Rev. Lett. **83**, 694 (1999).
[24] S. Kümmel, L. Kronik, and J. P. Perdew, Phys. Rev. Lett. **93**, 213002 (2004).
[25] T. Körzdörfer, M. Mundt, and S. Kümmel, Phys. Rev. Lett. **100**, 133004 (2008).
[26] R. Armiento, S. Kümmel, and T. Körzdörfer, Phys. Rev. B **77**, 165106 (2008).
[27] T. Körzdörfer and S. Kümmel, in *Self-interaction correction in the Kohn-Sham Framework*, edited by A. K. Roy, Theoretical and Computational Developments in Modern Density Functional Theory (Nova Science Publishers, New York, 2012).
[28] P. Duffy, D. P. Chong, M. E. Casida, and D. R. Salahub, Phys. Rev. A **50**, 4707 (1994).
[29] J. Akola, M. Manningen, H. Häkkinnen, U. Landman, X. Li, and L.-S. Wang, Phys. Rev. B **62**, 13216 (2000).
[30] D. P. Chong, O. V. Gritsenko, and E. J. Baerends, J. Chem. Phys. **116**, 1760 (2002).
[31] M. Mundt, S. Kümmel, B. Huber, and M. Moseler, Phys. Rev. B **73**, 205407 (2006).
[32] T. Körzdörfer, S. Kümmel, N. Marom, and L. Kronik, Phys. Rev. B **79**, 201205 (2009).

[33] T. Korzdorfer, S. Kummel, N. Marom, and L. Kronik, Phys. Rev. B **82**, 129903 (2010).
[34] U. Salzner and R. Baer, J. Chem. Phys. **131**, 231101 (2009).
[35] M. Dauth, T. Körzdörfer, S. Kümmel, J. Ziroff, M. Wiessner, A. Schöll, F. Reinert, M. Arita, and K. Shimada, Phys. Rev. Lett. **107**, 193002 (2011).
[36] L. Kronik and S. Kümmel, Gas-Phase Valence-Electron Photoemission Spectroscopy Using Density Functional Theory, in *Top. Curr. Chem. First Princ. Approaches to Spectrosc. Prop. Complex Mater*, edited by C. di Valentin, S. Botti, and M. Coccoccioni, 347 ed. (Springer, Berlin, 2014), pp. 137–192.
[37] A. Dreuw, J. L. Weisman, and M. Head-Gordon, J. Chem. Phys. **119**, 2943 (2003).
[38] D. J. Tozer, J. Chem. Phys. **119**, 12697 (2003).
[39] N. T. Maitra, J. Chem. Phys. **122**, 234104 (2005).
[40] D. Hofmann, T. Körzdörfer, and S. Kümmel, Phys. Rev. Lett. **108**, 146401 (2012).
[41] C. Toher, A. Filippetti, S. Sanvito, and K. Burke, Phys. Rev. Lett. **95**, 146402 (2005).
[42] S.-H. Ke, H. U. Baranger, and W. Yang, J. Chem. Phys. **126**, 201102 (2007).
[43] Z.-F. Liu, J. P. Bergfield, K. Burke, and C. A. Stafford, Phys. Rev. B **85**, 155117 (2012).
[44] D. Hofmann and S. Kümmel, Phys. Rev. B **86**, 201109 (2012).
[45] J. P. Perdew and A. Zunger, Phys. Rev. B **23**, 5048 (1981).
[46] J. P. Perdew, Chem. Phys. Lett. **64**, 127 (1979).
[47] T. Körzdörfer, S. Kümmel, and M. Mundt, J. Chem. Phys. **129**, 014110 (2008).
[48] D. Hofmann and S. Kümmel, J. Chem. Phys. **137**, 064117 (2012).
[49] J. P. Perdew, R. G. Parr, M. Levy, and J. L. J. Balduz, Phys. Rev. Lett. **49**, 1691 (1982).
[50] A. J. Cohen, P. Mori-Sánchez, and W. Yang, Science **321**, 792 (2008).
[51] T. Stein, J. Autschbach, N. Govind, L. Kronik, and R. Baer, J. Phys. Chem. Lett. **3**, 3740 (2012).
[52] E. Kraisler and L. Kronik, Phys. Rev. Lett. **110**, 126403 (2013).
[53] P. Mori-Sánchez, A. J. Cohen, and W. Yang, Phys. Rev. Lett. **100**, 146401 (2008).
[54] P. Mori-Sánchez, A. J. Cohen, and W. Yang, Phys. Rev. Lett. **102**, 066403 (2009).
[55] E. Kraisler and L. Kronik, J. Chem. Phys. **140**, 18A540 (2014).
[56] E. Kraisler, T. Schmidt, S. Kümmel, and L. Kronik, J. Chem. Phys. **143**, 104105 (2015).
[57] O. A. Vydrov and G. E. Scuseria, J. Chem. Phys. **125**, 234109 (2006).
[58] A. Ruzsinszky, J. P. Perdew, G. I. Csonka, O. A. Vydrov, and G. E. Scuseria, J. Chem. Phys. **126**, 104102 (2007).
[59] E. Kraisler and L. Kronik, Phys. Rev. A **91**, 032504 (2015).
[60] S. Kümmel and L. Kronik, Rev. Mod. Phys. **80**, 3 (2008).
[61] A. Ruzsinszky, J. P. Perdew, G. I. Csonka, G. E. Scuseria, and O. A. Vydrov, Phys. Rev. A **77**, 060502 (2008).
[62] A. D. Becke, J. Chem. Phys. **98**, 1372 (1993).
[63] A. D. Becke, J. Chem. Phys. **98**, 5648 (1993).
[64] J. P. Perdew, M. Ernzerhof, and K. Burke, J. Chem. Phys. **105**, 9982 (1996).
[65] M. Ernzerhof, Chem. Phys. Lett. **263**, 499 (1996).
[66] M. Ernzerhof, J. P. Perdew, and K. Burke, Int. J. Quantum Chem. **64**, 285 (1997).
[67] K. Burke, M. Ernzerhof, and J. P. Perdew, Chem. Phys. Lett. **265**, 115 (1997).
[68] F. G. Cruz, K.-C. Lam, and K. Burke, J. Phys. Chem. A **102**, 4911 (1998).
[69] J. Jaramillo, G. E. Scuseria, and M. Ernzerhof, J. Chem. Phys. **118**, 1068 (2003).
[70] B. G. Janesko and G. E. Scuseria, J. Chem. Phys. **127**, 164117 (2007).
[71] J. P. Perdew, V. N. Staroverov, J. Tao, and G. E. Scuseria, Phys. Rev. A **78**, 052513 (2008).
[72] K. Burke, F. G. Cruz, and K.-C. Lam, J. Chem. Phys. **109**, 8161 (1998).
[73] A. V. Arbuznikov and M. Kaupp, J. Chem. Phys. **141**, 204101 (2014).
[74] B. G. Janesko and G. E. Scuseria, J. Chem. Phys. **128**, 084111 (2008).
[75] H. Bahmann, A. Rodenberg, A. V. Arbuznikov, and M. Kaupp, J. Chem. Phys. **126**, 011103 (2007).
[76] A. V. Arbuznikov and M. Kaupp, Chem. Phys. Lett. **440**, 160 (2007).
[77] M. Kaupp, H. Bahmann, and A. V. Arbuznikov, J. Chem. Phys. **127**, 194102 (2007).
[78] A. V. Arbuznikov, H. Bahmann, and M. Kaupp, J. Phys. Chem. A **113**, 11898 (2009).
[79] R. Haunschild, B. G. Janesko, and G. E. Scuseria, J. Chem. Phys. **131**, 154112 (2009).
[80] K. Theilacker, A. V. Arbuznikov, H. Bahmann, and M. Kaupp, J. Phys. Chem. A **115**, 8990 (2011).
[81] A. V. Arbuznikov and M. Kaupp, Int. J. Quantum Chem. **111**, 2625 (2011).
[82] A. V. Arbuznikov and M. Kaupp, J. Chem. Phys. **136**, 014111 (2012).
[83] E. R. Johnson, J. Chem. Phys. **141**, 124120 (2014).
[84] P. de Silva and C. Corminboeuf, J. Chem. Phys. **142**, 074112 (2015).
[85] R. Haunschild and G. E. Scuseria, J. Chem. Phys. **132**, 224106 (2010).
[86] T. M. Maier, H. Bahmann, and M. Kaupp, J. Chem. Theory Comput. **11**, 4226 (2015).
[87] A. V. Arbuznikov, M. Kaupp, and H. Bahmann, J. Chem. Phys. **124**, 204102 (2006).
[88] T. Schmidt, E. Kraisler, A. Makmal, L. Kronik, and S. Kümmel, J. Chem. Phys. **140**, 18A510 (2014).
[89] T. Schmidt, E. Kraisler, L. Kronik, and S. Kümmel, Phys. Chem. Chem. Phys. **16**, 14357 (2014).
[90] C. Adamo and V. Barone, J. Chem. Phys. **110**, 6158 (1999).
[91] M. Ernzerhof and G. E. Scuseria, J. Chem. Phys. **110**, 5029 (1999).
[92] N. Sai, P. F. Barbara, and K. Leung, Phys. Rev. Lett. **106**, 226403 (2011).
[93] Y. Imamura, R. Kobayashi, and H. Nakai, Chem. Phys. Lett. **513**, 130 (2011).
[94] V. Atalla, M. Yoon, F. Caruso, P. Rinke, and M. Scheffler, Phys. Rev. B **88**, 165122 (2013).
[95] J. Janak, Phys. Rev. B **18**, 7165 (1978).
[96] M. Levy, J. P. Perdew, and V. Sahni, Phys. Rev. A **30**, 2745 (1984).
[97] C.-O. Almbladh and U. von Barth, Phys. Rev. B **31**, 3231 (1985).
[98] J. P. Perdew and M. Levy, Phys. Rev. B **56**, 16021 (1997).

[99] O. V. Gritsenko, B. Braïda, and E. J. Baerends, J. Chem. Phys. **119**, 1937 (2003).
[100] T. Körzdörfer and S. Kümmel, Phys. Rev. B **82**, 155206 (2010).
[101] T. Körzdörfer, J. Chem. Phys. **134**, 094111 (2011).
[102] N. Marom, F. Caruso, X. Ren, O. T. Hofmann, T. Körzdörfer, J. R. Chelikowsky, A. Rubio, M. Scheffler, and P. Rinke, Phys. Rev. B **86**, 245127 (2012).
[103] T. Grabo, T. Kreibich, and E. K. U. Gross, Mol. Eng. **7**, 27 (1997).
[104] See Supplemental Material at http://link.aps.org/supplemental/10.1103/PhysRevB.93.165120 for details on the evaluation of Eq. (12), a direct comparison of KS eigenvalues for ISO and ISOII obtained with and without pseudopotentials, and the extended versions of Figs. 6 and 7.
[105] D. Hofmann, S. Klüpfel, P. Klüpfel, and S. Kümmel, Phys. Rev. A **85**, 062514 (2012).
[106] R. Haunschild, T. M. Henderson, C. A. Jiménez-Hoyos, and G. E. Scuseria, J. Chem. Phys. **133**, 134116 (2010).
[107] V. Vlček, H. R. Eisenberg, G. Steinle-Neumann, L. Kronik, and R. Baer, J. Chem. Phys. **142**, 034107 (2015).
[108] A. Makmal, S. Kümmel, and L. Kronik, J. Chem. Theory Comp. **5**, 1731 (2009).
[109] A. Makmal, S. Kümmel, and L. Kronik, J. Chem. Theory Comput. **7**, 2665 (2011).
[110] Bond lengths used in this publication: $R_{\mathrm{BeH}} = 2.5368$ bohr, $R_{\mathrm{CO}} = 2.1322$ bohr, $R_{\mathrm{NN}} = 2.0743$ bohr and $R_{\mathrm{NO}} = 2.1746$ bohr. All values are taken from *CRC Handbook of Chemistry and Physics*, 92th ed., edited by D. R. Lide (CRC, London, 2011), available on http://www.hbcpnetbase.com.
[111] J. B. Krieger, Y. Li, and G. J. Iafrate, Phys. Rev. A **46**, 5453 (1992).
[112] G. J. Iafrate and J. B. Krieger, J. Chem. Phys. **138**, 094104 (2013).
[113] L. Kronik, A. Makmal, M. L. Tiago, M. M. G. Alemany, M. Jain, X. Huang, Y. Saad, and J. R. Chelikowsky, Phys. Status Solidi **243**, 1063 (2006).
[114] N. Troullier and J. L. Martins, Phys. Rev. B **43**, 1993 (1991).
[115] E. Engel, A. Hock, R. N. Schmid, R. M. Dreizler, and N. Chetty, Phys. Rev. B **64**, 125111 (2001).
[116] F. Gygi, Phys. Rev. B **48**, 11692 (1993).
[117] J. P. Perdew, S. Kurth, A. Zupan, and P. Blaha, Phys. Rev. Lett. **82**, 2544 (1999).
[118] R. Stowasser and R. Hoffmann, J. Am. Chem. Soc. **121**, 3414 (1999).
[119] S.-Y. Liu, K. Alnama, J. Matsumoto, K. Nishizawa, H. Kohguchi, Y.-P. Lee, and T. Suzuki, J. Phys. Chem. A **115**, 2953 (2011).
[120] N. Kishimoto and K. Ohno, J. Phys. Chem. A **104**, 6940 (2000).
[121] R. Boschi, J. N. Murrell, and W. Schmidt, Faraday Discuss. Chem. Soc. **54**, 116 (1972).
[122] As a general remark we note that, unfortunately, there is presently no way known how to *a priori* determine the functional parameter such that $-\varepsilon_{\mathrm{ho}} = IP$ universally.
[123] J. Sauther, J. Wüsten, S. Lach, and C. Ziegler, J. Chem. Phys. **131**, 034711 (2009).
[124] S. Kera, S. Tanaka, H. Yamane, D. Yoshimura, K. Okudaira, K. Seki, and N. Ueno, Chem. Phys. **325**, 113 (2006).
[125] N. L. Nguyen, G. Borghi, A. Ferretti, I. Dabo, and N. Marzari, Phys. Rev. Lett. **114**, 166405 (2015).
[126] P. Puschnig, S. Berkebile, A. J. Fleming, G. Koller, K. Emtsev, T. Seyller, J. D. Riley, C. Ambrosch-Draxl, F. P. Netzer, and M. G. Ramsey, Science **326**, 702 (2009).
[127] M. Dauth, M. Wiessner, V. Feyer, A. Schöll, P. Puschnig, F. Reinert, and S. Kümmel, New J. Phys. **16**, 103005 (2014).
[128] O. V. Vydrow and G. E. Scuseria, J. Chem. Phys. **121**, 8187 (2004); **122**, 184107 (2005).
[129] Note that the strength of the electrical field is a factor of two larger in our figure than in the one of Ref. [44] since Ref. [44] erroneously missed a factor two in the conversion of the atomic units.